Soil Structure Interaction Problems: Impedance of Piled Foundations in Saturated Soils

Muhammad Matanov
Karshi State University PhD student
Karshi, Uzbekistan
mm939011166@gmail.com
https://orcid.org/0009-0008-8858-5010

Abstract: This article examines the dynamic impedance of single piles and pile groups in water-saturated soils using a 3D boundary element method (BEM) based on Biot's two-phase poroelastic theory. Unlike prior studies treating soils as elastic or viscoelastic, this approach models them as fluid-saturated, poroelastic materials and piles as elastic or viscoelastic solids, enabling detailed pile-soil interaction analysis. Validation is achieved through literature comparisons. Results reveal the effects of excitation frequency, soil permeability, and pile flexibility. Key findings highlight soil permeability's impact on horizontal impedance and wave propagation, along with increased foundation stiffness in saturated soils at low frequencies. The study exposes single-phase model limitations and demonstrates the proposed method's versatility for complex foundation analysis.

Keywords: *Dynamic impedance, boundary element method (BEM), poroelastic soils, pile foundations, soil-structure interaction, Biot's theory, saturated soils, pile-soil interaction, wave propagation, foundation stiffness.*

1. Introduction

This article outlines the governing equations and numerical procedure for calculating the dynamic impedance of piled foundations in water-saturated soils. It reviews previous techniques, discusses the coupled BEM model's adaptation, and validates it with existing studies. Most research focuses on pile displacements under harmonic loads in semi-spaces, typically modeling soil as elastic or viscoelastic, with few considering water-saturated soils. Biot's two-phase theory, which accounts for compressibility, fluid viscosity, and solid-fluid interaction, is rarely used.

This study uses a 3D BEM to determine the dynamic impedance of piles and pile groups in poroelastic soils. Piles are modeled as elastic or viscoelastic solids, and soil as a fluid-filled poroelastic medium. Unlike earlier methods, this approach demands more computation but offers greater accuracy and versatility, allowing for complex pile geometries, including inclined piles and varied cross-sections, as well as different pile-soil contact conditions. While the results focus on a semi-space, the method extends to more complex subsurface geometries, presenting vertical and horizontal impedance results and analyzing the effects of excitation frequency, pile flexibility, and poroelastic properties.

2. Application of the Coupled BEM Model to the problem. System of equations to be solved.

The proposed model is able to work with elastic and viscoelastic regions (piles), poroelastic regions (soil) and takes into account the interaction between them at the soil-pile interface. It is also possible to use unbounded regions using a reasonable number of unknowns and to represent radiation damping.

The soil is considered as a poroelastic, fluid-filled, homogeneous and isotropic material governed by Biot's theory. The equations $\tau_{ij} = \left(\lambda + \dfrac{Q^2}{R}\right) e\delta_{ij} + 2\mu\varepsilon_{ij} + Q\varepsilon\delta_{ij}$, $\tau = Qe + R\varepsilon$ therefore constitute the law of behavior of this material. For a harmonic excitation in time of the type $e^{i\omega t}$ ($\omega =$ angular frequency) the equations

$$\mu\nabla^2 u + (\lambda+\mu)\nabla e + \left(\frac{Q}{R} - \frac{\hat{\rho}_{12}}{\hat{\rho}_{22}}\right)\nabla\tau + \left(\frac{\hat{\rho}_{11}\hat{\rho}_{22} - \hat{\rho}_{12}^2}{\hat{\rho}_{22}}\right)\omega^2 u +$$

$$+ X - \frac{\hat{\rho}_{12}}{\hat{\rho}_{22}} X' = 0,$$

$$\nabla^2\tau + \omega^2\frac{\hat{\rho}_{22}}{R}\tau + \omega^2\frac{\hat{\rho}_{22}}{R}\tau + \omega^2\left(\hat{\rho}_{12} - \frac{Q}{R}\hat{\rho}_{22}\right)e + \nabla X' = 0$$

where $\hat{\rho}_{11} = \rho_{11} - i\dfrac{b}{\omega}$; $\hat{\rho}_{22} = \rho_{22} - i\dfrac{b}{\omega}$; $\hat{\rho}_{12} = \rho_{12} + i\dfrac{b}{\omega}$; correspond to the governing equations in the frequency domain as a function of the solid displacements and the stress in the fluid. The integral formulation of the governing equations for this medium is given by the expressions $u_j^k + \int_\Gamma t_{ji}^* u_i d\Gamma - \int_\Gamma U_{nj}^* \tau d\Gamma = \int_\Gamma u_{ji}^* t_i d\Gamma - \int_\Gamma \tau_j^* U_n d\Gamma$ and $-J\tau^k + \int_\Gamma t_{oi}^* u_i d\Gamma - \int_\Gamma \left(U_{no}^* - JX_i'^* n_i\right)\tau d\Gamma = \int_\Gamma u_{oi}^* t_i d\Gamma - \int_\Gamma \tau_o^* U_n d\Gamma.$

Applying the procedure described to numerically solve these equations using the boundary element method, the above equations can be written in a condensed form as:

$$c^k u^k + \int_\Gamma p^* u d\Gamma = \int_\Gamma u^* p d\Gamma \tag{1}$$

where, u and p are vectors containing the variables in the contour:

$$u = \begin{Bmatrix} u_1 \\ u_2 \\ u_3 \\ \tau \end{Bmatrix}, \quad p = \begin{Bmatrix} t_1 \\ t_2 \\ t_3 \\ U_n \end{Bmatrix} \tag{2}$$

u^* and p^* are the tensors of the fundamental solution whose terms appear in the table $\nabla^2 p - \nabla X' = \dfrac{1}{c^2}\ddot{p}$ and in the:

$$u^* = \begin{bmatrix} u_{11}^* & u_{12}^* & u_{13}^* & -\tau_1^* \\ u_{21}^* & u_{22}^* & u_{33}^* & -\tau_2^* \\ u_{31}^* & u_{32}^* & u_{33}^* & -\tau_3^* \\ u_{o1}^* & u_{o2}^* & u_{o3}^* & -\tau_o^* \end{bmatrix}, \quad p^* = \begin{bmatrix} t_{11}^* & t_{12}^* & t_{13}^* & -U_{n1}^* \\ t_{21}^* & t_{22}^* & t_{33}^* & -U_{n2}^* \\ t_{31}^* & t_{32}^* & t_{33}^* & -U_{n3}^* \\ t_{o1}^* & t_{o2}^* & t_{o3}^* & -\hat{U}_{no}^* \end{bmatrix} \tag{3}$$

and c^k is the local free term at the placement point x_k of the form:

$$c^k = \begin{bmatrix} c_{11}^e & c_{12}^e & c_{13}^e & 0 \\ c_{21}^e & c_{22}^e & c_{33}^e & 0 \\ c_{31}^e & c_{32}^e & c_{33}^e & 0 \\ 0 & 0 & 0 & Jc^p \end{bmatrix} \tag{4}$$

where c_{ij}^{e} are equal to the free terms of the elastostatic equations at the placement point x_k and c^p are equal to the scalar static term in x_k.

The discretization into boundary elements of equation (1) leads to a system of $4N$ equations:

$$Nu = Gp \tag{5}$$

where N is the number of nodes on the boundary; u is a vector containing the solid displacements and fluid stresses at the boundary nodes; p is a vector containing the solid stresses and fluid normal displacements at the boundary nodes; and N, G are the dimension system matrices $4N \times 4N$ obtained by integration over the boundary elements of the 3D time-harmonic fundamental solution for poroelastic media using the shape functions.

The piles are modeled with their real geometry as a continuous, homogeneous, isotropic, linear and viscoelastic medium. The equations $\mu\nabla^2 u + (\lambda + \mu)\nabla e + X = -\rho\omega^2 u$ assume a harmonic displacement in time of the type $u(x,t) = u(x;\omega)e^{i\omega t}$. The variables are understood to be position- and frequency-dependent. They constitute the governing equation in the frequency domain. The integral representation of the displacements on the boundary is given by the equation $u_j^k + \int_\Gamma t_{ji}^* u_i d\Gamma = \int_\Gamma t_{ji}^* t_i d\Gamma$, where in this case u and p are the displacement and stress vectors, respectively, on the pile boundary, and u^* and p^* are the tensors of the fundamental solution of displacements and stresses, respectively. A boundary element equation per pile leads to a system with $3N^p$ equations:

$$N^p u^p = G^p p^p \tag{6}$$

where N^p is the number of nodes on the boundary; u^p and p^p are vectors containing the displacements and stresses respectively of the nodes of the boundary; and N^p, G^p are the matrices of the system of dimensions $3N^p \times 3N^p$ obtained by integration over the elements of the boundary of the fundamental harmonic solution in 3D time for elastic media ($u_{lk}^*(x,\xi,\omega) = \frac{1}{4\pi\mu}(\psi\delta_{lk} - \chi r_l r_k)$ and $t_{lk}^*(x,\xi,\omega) = = \frac{1}{4\pi}\left[\frac{\partial r}{\partial n}(A\delta_{lk} + B r_l r_k) + (A r_l n_l + C r_l n_k)\right]$ using the shape functions.

Equation (5) represents the poroelastic soil (nodes on the free surface and pile boundary), and equation (6) corresponds to each pile. The equations are coupled through equilibrium and compatibility conditions at the pile-soil interfaces, with the contact considered fully welded. The hydraulic boundary condition at the contact surface is an intermediate case between fully drained (permeable pile) and impermeable (impermeable pile).

The equilibrium and compatibility conditions between the poroelastic biphasic region and the impermeable viscoelastic pile (indicated by the superscript p) are as follows:

Balance:

$$t_n^p + (t_n + \tau) = 0, \quad t_t^p + t_t = 0 \tag{7}$$

where the subscripts n and t indicate the normal and tangential components, respectively.

Compatibility:

$$u_n^p = u_n = U_n, \quad u_t^p = u_t \tag{8}$$

If the solid material is permeable, the condition of normal fluid displacement in the pore must be replaced by a pore pressure condition: in this case the above equations become as follows:

Balance:

$$t_n^p + t_n = 0, \; t_t^p + t_t = 0, \; \tau = 0 \tag{9}$$

Compatibility:

$$u_n^p = u_n, \; u_t^p = u_t \tag{10}$$

In this study the free surface of the soil is considered drained.

To visualize the assembly process of the coupled pile-soil system, let us look at a very simple case, which corresponds to a simple pile embedded in a poroelastic semi-space. The boundary element equation for each region (pile and soil) in a divided form according to the contours indicated in figure 1 are:

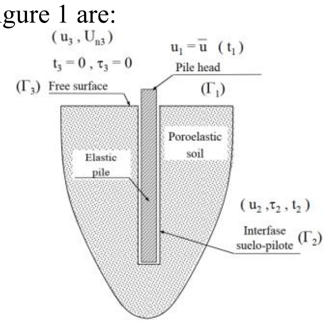

Figure 1. Impermeable pile in a poroelastic half-space: Boundary conditions and unknowns in coupled equations.

Elastic pile:

$$N_1^p u_1^p + N_2^p u_2^p = G_1^p t_1^p + G_2^p t_2^p \tag{11}$$

Poroelastic soil:

$$\begin{bmatrix} N_2^{ss} & N_2^{sw} \\ N_2^{ws} & N_2^{ww} \end{bmatrix} \begin{Bmatrix} u_2 \\ \tau_2 \end{Bmatrix} + \begin{bmatrix} N_3^{ss} & N_3^{sw} \\ N_3^{ws} & N_3^{ww} \end{bmatrix} \begin{Bmatrix} u_3 \\ \tau_3 \end{Bmatrix} = = \begin{bmatrix} G_2^{ss} & G_2^{sw} \\ G_2^{ws} & G_2^{ww} \end{bmatrix} \begin{Bmatrix} t_2 \\ U_{n2} \end{Bmatrix} + \begin{bmatrix} G_3^{ss} & G_3^{sw} \\ G_3^{ws} & G_3^{ww} \end{bmatrix} \begin{Bmatrix} t_3 \\ U_{n3} \end{Bmatrix} \tag{12}$$

where the subscripts 1, 2, and 3 correspond to the boundary in contact with the pile cap at which the nodal displacement values are known (G_1) , to the pile-soil interface (G_2) , and to the tension-free soil surface (G_3) respectively. Substituting in (11) and (12) the equilibrium and compatibility conditions along the pile-soil interface and the external boundary conditions, the combined equations for the coupled dynamic problem become:

$$\begin{bmatrix} -G_1^p & N_2^p & -G_2^p n_2 & G_2^p & 0 & 0 \\ 0 & N_2^{ss} + G_2^{sw} n_2 & N_2^{sw} & G_2^{ss} & N_3^{ss} & G_3^{sw} \\ 0 & N_2^{ws} + G_2^{ww} n_2 & N_2^{ww} & G_2^{ws} & N_3^{ws} & G_3^{ww} \end{bmatrix} \begin{Bmatrix} t_1^p \\ u_2 \\ \tau_2 \\ t_2 \\ u_3 \\ U_{n3} \end{Bmatrix} = \begin{Bmatrix} -N_1^p \bar{u}_1 \\ 0 \\ 0 \end{Bmatrix} \tag{13}$$

where u_2 (displacement vector of the solid skeleton/pile), τ_2 (stress in the poroelastic soil fluid), and t_2 (stress vectors in the solid skeleton) are the unknown nodal values at the pile-soil interface (G_2) , with n_2 as a unit vector normal to the pile boundary. Equations for permeable contact are omitted for brevity.

To validate the model, pile and pile group impedances are compared with literature results. The dynamic stiffness matrix K_{ij} relates forces (and moments) at the pile head to resulting displacements (and rotations). For a pile group, all heads are constrained by a rigid cap, and foundation stiffness is the sum of individual contributions. Figure 2 illustrates the problem. More complex foundations (e.g., unequal, inclined, or variable-section piles) require only a boundary mesh modification, not changes to the technique.

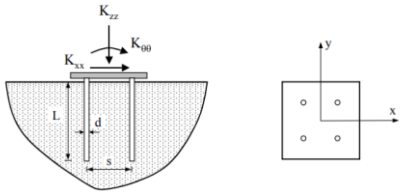

Figure 2. Group of piles 2×2 embedded in a semi-space. Definition of the geometry of the problem.

For harmonic excitation the dynamic stiffness terms are functions of frequency ω of the form:

$$K_{ij} = k_{ij} + i a_0 c_{ij} \tag{14}$$

where k_{ij} and c_{ij} are the dynamic stiffness's and damping coefficients, respectively, i the imaginary unit and a_o is the dimensionless frequency given by:

$$a_o = \frac{\omega d}{c_s} \tag{15}$$

where c_s is the speed of propagation of the shear wave in the ground and d is the diameter of the pile.

3. Piles embedded in a viscoelastic semi-space. Piles embedded in a fluid-filled poroelastic semi-space.

Figure 3 compares the lateral impedances (real and imaginary parts) of a single pile and a group of piles 2×2 embedded in a homogeneous isotropic and viscoelastic semi-space using the indicated technique with those of Kaynia & Kausel. These authors consider piles as prismatic elements with elastic and linear behavior, while the soil is a semi-infinite viscoelastic medium using the Green function via the Thin Layer Method.

Piles are treated as a uniform continuous medium with elastic behavior, and the surrounding soil as a uniform viscoelastic medium with an internal damping coefficient $\beta = 0.05$. The elasticity modulus ratio is $E_p / E = 10^3$, the density ratio is $\rho / \rho_p = 0.7$, and Poisson's ratios are $\nu = 0.4$ for soil and $\nu_p = 0.25$ for piles. The pile's aspect ratio L/d is 15.

Impedance functions for different ratios s/d (separation between piles) are normalized using the static stiffness of a single pile (K_{xxo}) and the number of piles (N). Results are plotted against the dimensionless frequency from equation (15).

Figure 3 shows close agreement for single piles and 2×2 groups with $s/d = 5$ and 10. For $s/d = 2$, the proposed method shows a slightly higher real part as frequency increases. This discrepancy from Kaynia & Kausel was also noted by Sen, Davies, & Banerjee for a 3×3 group with the same pile spacing.

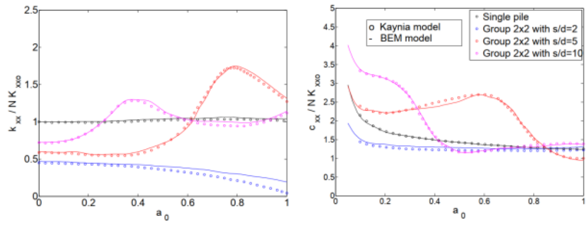

Figure 3. Horizontal impedance of a single pile and a 2×2 pile group in viscoelastic soil: Comparison with Kaynia.

The dynamic impedance of the group is not the product of an isolated pile's impedance and the number of piles in the cap. Each pile is affected not only by its own load but also by the load and deformation of nearby piles. This pile-soil-pile interaction effect is frequency-dependent and arises from waves generated at the periphery of each pile, which propagate through the soil to nearby piles.

In this case the results are compared with those obtained by Zeng & Rajapakse concerning the vertical impedance of a simple pile embedded in a poroelastic half-space. The properties of the soil, considered as a two-phase poroelastic medium, have been taken from Zeng & Rajapakse. The dimensionless values adopted, whose definition is given below, are: $\lambda^* = 1.5$, $Q^* = 2.87$, $R^* = 2.83$, $\rho_s^* = 1.44$, $\rho_f^* = 0.53$, $\rho_a^* = 0$. In addition, two different values of permeability have been taken into account, which correspond to the values of the dimensionless dissipation constant $b^* = 232.15$ and $b^* = 0$ respectively. The porosity of the medium is in all cases $\phi = 0.482$. The meaning of the dimensionless variables is as follows:

$$\lambda^* = \frac{\lambda}{\mu}, \quad \rho_s^* = \frac{\rho_s}{\rho}, \quad \rho_f^* = \frac{\rho_f}{\rho}, \quad \rho_a^* = \frac{\rho_a}{\rho}. \tag{16}$$

$$Q^* = \frac{Q}{\mu}, \quad R_s^* = \frac{R}{\rho}, \quad b^* = \frac{bd}{\sqrt{\mu\rho}}. \tag{17}$$

where $\rho = (1-\phi)\rho_s + \phi\rho_f$ is the density of the homogeneous material, μ is the transverse rigidity modulus of the drained solid skeleton and d is the diameter of the pile.

The pile is modeled as elastic and impermeable with: flexibility ratio $E_p / E = 10^3$, density ratio $\rho_p / \rho = 1.2$, Poisson's ratio $\nu_p = 0.3$ and Aspect ratio $L/d = 10$.

Illustrates the normalized vertical stiffness (real and imaginary parts) relative to the static stiffness K_{zzo} for fully drained elastic soil. The dimensionless frequency is defined by equation (15), where c_s is the shear wave propagation speed in the homogeneous material.

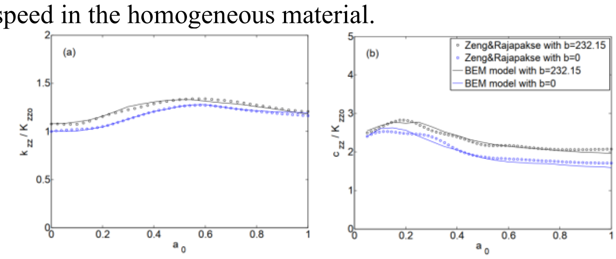

Figure 4. Vertical impedance of a single pile in a poroelastic medium: Comparison with Zeng & Rajapakse.

The results show that both results coincide. It is also observed that both the stiffness and the damping (real and imaginary parts respectively) increase with b^* (less permeable media). This effect of soil permeability on dynamic impedance is studied in greater depth in the following section.

4. Numerical analysis and discussion of results

This section evaluates dynamic impedances of piles in a saturated poroelastic half-space. Properties of the porous medium: $\lambda^*=1$, $Q^*=14.33$, $R^*=7.72$, $\rho_s^*=1.12$, $\rho_f^*=0.78$, $\rho_a^*=0$, $b^*=59.30$, porosity $\phi=0.35$ and skeleton damping $\beta=0.05$.

Piles exhibit viscoelastic behavior with: Flexibility ratio $E_p/E=343$ (E: modulus of drained poroelastic medium), Density ratio $\rho_p/\rho=1.94$, Poisson's ratio $\nu_p=0.2$, Damping coefficient $\beta=0$, Aspect ratio $L/d=15$.

Unless specified, pile-soil contact is assumed impermeable. Subsequent sections analyze the effects of excitation frequency, pile flexibility, soil permeability, and pile-soil contact on dynamic impedance.

4.1. Influence of pile flexibility (single pile)

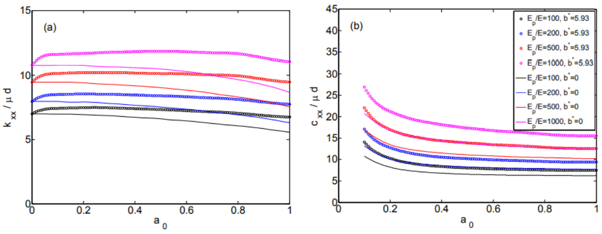

Figure 5: Influence of Pile Flexibility on Horizontal Impedance

The analysis examines the flexibility ratio E_p/E on k_{xx} and c_{xx} against dimensionless frequency a_o, for four values E_p/E = 100, 200, 500, 1000, and two poroelastic soils: $b^*=0\ (k\to\infty)$ and $b^*=5.93$. Key observations: Across the frequency range, k_{xx} and c_{xx} increase with E_p/E. For $b^*=5.93$, dynamic stiffness shows minimal dependence on a_o except at low frequencies, where stiffness aligns with static values.

For $b^*=0$, impedance and stiffness reduce significantly a a_o increases, with the effect amplified at higher E_p/E. Dynamic impedance for slenderness ratios $L/d=5,10,20$ was analyzed at $E_p/E=100,200,500$. Observations: Results are identical for $L/d=5,10,20$, Insensitivity above a critical slenderness L_a/d reflects pile deformation limited to depths $<L_a$, as predicted by stiffness ratios.

4.2. Influence of soil permeability (single pile and groups of piles)

High b values hinder fluid flow through the solid skeleton, affecting dynamic responses. Figure 6 illustrates the variation of S and P2 wave velocities versus b^* for three frequencies $(a_o=0.25,\ 0.5,\ 0.75)$ Velocities are normalized by c_s (shear wave velocity in undrained elastic conditions).

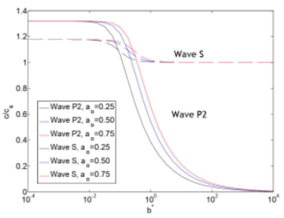

Figure 6. Amplitudes of wave propagation velocities in poroelastic soil versus dissipation constant.

Key Observations: P1: Speed $(|c_{p1}/c_s|\approx 8)$ reduces by ~1%, S: Speed varies ~20%, P2: Significant changes, with rapid growth for b^* between 10^1 and 10^{-2}.

Adopted b^* values: for $b^*>10$, permeability effects are minimal. Selected values: $b^*=59.3,\ 59.3\times10^{-2}$ and 59.3×10^{-4}

Figures 8 and 9 display changes in horizontal and vertical impedance for the selected b^* values. Both stiffness and damping decrease as b^* reduces, indicating higher permeability.

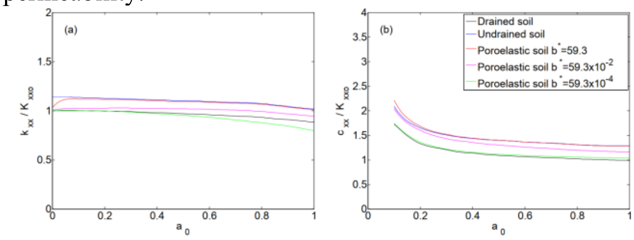

Figure 7. Influence of soil permeability. Horizontal impedance. Single pile.

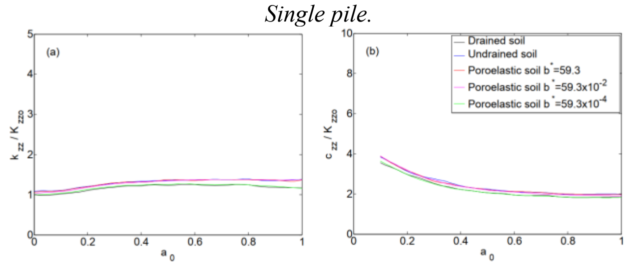

Figure 8. Influence of soil permeability. Vertical impedance. Single pile.

The figures show impedances for two limiting cases of the single-phase medium: drained and undrained elastic soil. High b^* causes behavior similar to an ideal undrained elastic soil, except at low frequencies. For vertical impedance, the drained elastic medium is the limiting value as permeability increases. Horizontal impedance drops below the drained elastic value at high permeability, increasing with a_o.

For vertical impedance in highly permeable soil, axial dynamic load transfers from the pile to the **poroelastic** soil via shear stresses in the solid skeleton. Here, fluid circulation between pores lacks rigidity, making the medium behave like drained soil. However, for horizontal impedance, lateral deflection transmits load to both soil phases, altering pore pressure and modifying behavior.

Figures 9 and 10 show horizontal and vertical impedances for 2×2 piles with $s/d=5$, while $s/d=10$ results appear in Figures 12 and 1. For $s/d=10$, the trend of increasing impedance with b^* continues, but wave reflection effects between piles create stiffness variations. Higher impedances can occur at smaller b^*. Figures 10a, 11a, and 12a show greater maximum stiffness for $b^*=59.3\times10^{-4}$ than $b^*=59.3\times10^{-2}$, shifting curves rightward as permeability increases.

This shift is due to higher permeability increasing wave velocity in the porous medium. Since velocity normalizing frequency a_o (in 15) corresponds to the S wave in an undrained medium (its lower limit), the horizontal stiffness of a highly permeable **poroelastic** medium can be lower than in drained elastic soil, as seen in Figure 10 1) a.

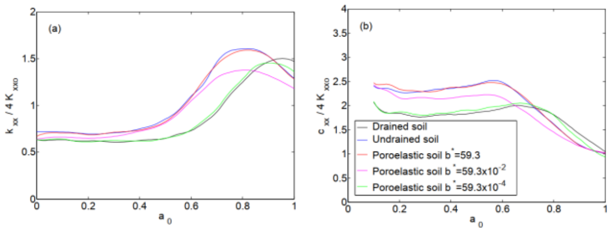

1) Horizontal impedance. Pile group 2×2 with $s/d=5$.

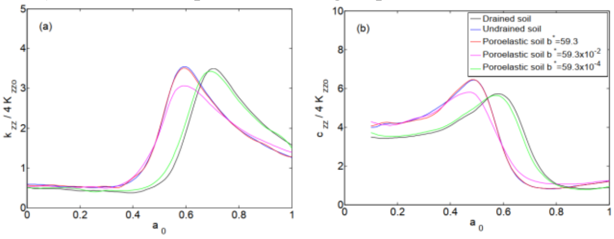

2) Vertical impedance. Pile group 2×2 with $s/d=5$.

Figure 9. Influence of soil permeability.

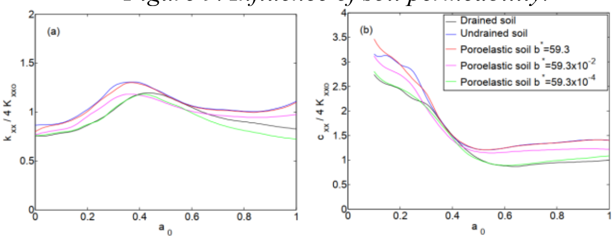

1) Horizontal impedance. Pile group 2×2 with $s/d=10$.

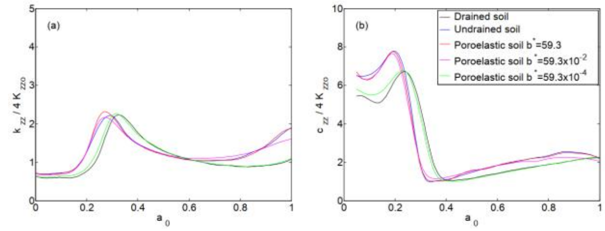

2) Vertical impedance. Pile group 2×2 with $s/d=10$.

Figure 10. Influence of soil permeability.

4.3. Influence of hydraulic boundary condition along the pile-soil interface (pile groups)

To study the hydraulic boundary condition effect, the impedance of a 2×2 pile group with $s/d=10$ was analyzed for two cases: completely impermeable contact (same normal displacement in both phases) and completely drained contact $(\tau=0)$. As expected, hydraulic influence increases as b^* decreases, confirmed by the results.

The influence is more noticeable in highly permeable soil $(b^*=59.3\times10^{-4})$, as seen in Figure 11. Impedance differences increase with a_o for $a_o=0.4$.

Stiffness for permeable contact is similar to ideal elastic drained soil, supporting the explanation for stiffness loss in saturated permeable soils due to the fluid phase. The curves also indicate foundation damping is insensitive to contact conditions.

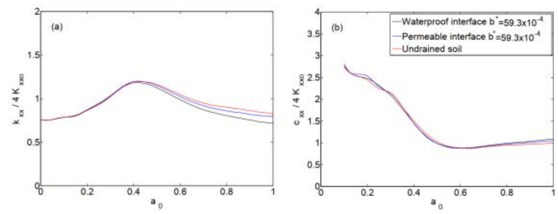

Figure 11. Influence of the hydraulic boundary on the pile-soil interface: Horizontal impedance of a 2×2 pile group with $s/d=10$ and $b^*=59.3\times10^{-4}$

5. Conclusions

This article presents a 3D boundary element method for calculating the dynamic stiffness of single piles and pile groups in two-phase poroelastic soils. Piles are modeled as elastic or viscoelastic solids, and the surrounding medium is a fluid-saturated poroelastic half-space. The method allows analysis of complex pile geometries and stratified soils, including poroelastic and viscoelastic zones. Vertical and horizontal impedances of cylindrical piles and 2×2 pile groups are computed, considering pile-soil interaction through equilibrium and compatibility conditions. Model validation is done through comparisons with existing studies.

Key findings show that foundation stiffness increases in saturated porous soils at low frequencies, influenced by permeability. The dissipation constant b, related to viscosity and permeability, impacts wave propagation and impedance. Highly permeable soils may reduce horizontal stiffness but have minimal effect on vertical stiffness. Pile group impedance is more frequency-dependent than single piles due to pile-soil interaction, which varies with spacing and soil properties. Pile-soil permeability mainly affects horizontal stiffness at very low b values.

Drained or undrained single-phase models may give unrealistic results depending on soil properties and foundation geometry. The proposed method, accounting for all material parameters, offers a more comprehensive and versatile approach than existing models.

References

[1] Kholmurodov A.E., Toshmurodova G. Singular solutions of one-dimensional SH wave equation in porous media. Siberial Electronic Mathematical Reports, 2016. 300-304-p

[2] Imomnazarov B.K, Mikhailov A.A., Khaydarov I.Q., Kholmurodov A.E. Численное решение задачи переноса растворенного вещества в пороупругом глинистом сланце. Siberial Electronic Mathematical Reports, 2021. 694-702-p.

[3] Leontovich M.A. Introduction to thermodynamics. Static physics: Textbook. Village - M.: Science. 1983.-416-p.

[4] Dorovsky V.N. Continuum theory of filtration // Geology and Geophysics. - 1989. - No. 7. - P. 39-45.

[5] Dorovsky V.N. Equations of continuum theory of filtration. Novosibirsk, 1987, 9 p. (Prepr / IGiG SB USSR Academy of Sciences, No. 9)

[6] Khalatnikov I.M. Theory of superfluidity. - M.: Nauka, 1971.– 320 p.

[7] Kholmurodov A.E., Imomnazarov Kh.Kh. Direct and inverse dynamic problems for the equation of SH waves in a porous medium//Bulletin of NUUz, series mechanics-mathematics, 2006, No.2, pp. 86-91. (01.00.00, No.8)

[8] Kholmuradov A.E., Imomnazarov Kh.Kh. Direct and inverse dynamic problems for SH-waves in porous media//Mathematical and Computer Modelling, V.45, Issues 3-4, 2007, pp. 270-280. (№1.Web of Science. IF=1.602)

[9] Matanov M. (2024) Formation of wave equations in elastic and porous elastic media by the boundary element method. News of KarSU 2024 (1) 52-61.

[10] Propagation of harmonic plane waves in an elastic half-space. Field equations A Xolmurodov, M Matanov, M Quzratov AIP Conference Proceedings 3244 (1)

[11] Xolmurodov A., Matanov M., Quzratov M. (2024) Reflection of SV waves in the elastic half-space. Field equations for angles of incidence less than the critical one News of KarSU 2024 4(2) 53-61